

Comprehensive Constraints on ALP Couplings from future e^+e^- Colliders, Muon $g - 2$, Thermal Dark Matter and Higgs Measurements

Pramod Sharma^{a,b}, Soham Singh^{b,c}, Mukesh Kumar^b, Ashok Goyal^{b,d}

^aIndian Institute of Science Education and Research Knowledge City Sector 81 S. A. S. Nagar Manauli PO 140306 Punjab India.

^bSchool of Physics and Institute for Collider Particle Physics University of the Witwatersrand Johannesburg Wits 2050 South Africa.

^cDepartment of Physics & Astronomy National Institute of Technology Rourkela 769 008 India.

^dDepartment of Physics & Astrophysics University of Delhi Delhi 110 007 India.

Abstract

In this article, we present projected 95% C.L. limits on Axion-Like Particle (ALP) couplings from ALP production at a future e^+e^- collider operating at $\sqrt{s} = 250$ GeV with integrated luminosity $L = 0.5 \text{ ab}^{-1}$. We constrain the effective couplings $g_{\gamma\gamma}$, $g_{Z\gamma}$, g_{ZZ} , and g_{WW} over the ALP mass range $20 \text{ GeV} \leq m_a \leq 100 \text{ GeV}$, finding projected bounds at the level of $O(10^{-1}) \text{ TeV}^{-1}$ for $g_{\gamma\gamma}/f_a$. We then focus on the 4σ -favored region of the muon anomalous magnetic moment Δa_μ , deriving corresponding bounds on $g_{\gamma\gamma}$ and the ALP–muon coupling $C_{\mu\mu}$, and applying them to a fermionic dark matter scenario in which the relic density depends on both m_χ and m_a . The same parameter space is further constrained by Higgs signal strength measurements through $h \rightarrow \gamma\gamma$ and $h \rightarrow Z\gamma$. A comparative analysis with existing experimental and theoretical bounds highlights the complementarity of Δa_μ , dark matter, and Higgs signal strengths observables in constraining ALP couplings.

Keywords: Axion-Like Particles, Future e^+e^- collider, Beyond the Standard Model

1. Introduction

Axion-like particles (ALPs) have emerged as a compelling framework for addressing multiple unresolved questions in particle physics. In addition to their origin as pseudo-Nambu-Goldstone bosons of broken global symmetries [1, 2], they offer phenomenological richness across various energy scales. For instance, ALPs have been invoked to help resolve the long-standing discrepancy in the muon’s anomalous magnetic moment Δa_μ [3], and when coupled to fermionic dark matter (DM), can enable thermal freeze-out consistent with the observed relic density [4]. Furthermore, loop-induced ALP couplings to electroweak Standard Model (SM) gauge bosons can modify Higgs-boson (h) decay rates, potentially accounting for mild excesses observed in $h \rightarrow \gamma\gamma$ and $h \rightarrow Z\gamma$ channels at the Large Hadron Collider (LHC) [5–7].

In this article, we intend to present and compare constraints on ALP couplings to electroweak gauge boson pairs ($V = W^\pm, Z, \gamma$) in the mass range $20 \text{ GeV} \leq m_a \leq 100 \text{ GeV}$. Our primary focus is on results from a dedicated analysis at future e^+e^- colliders, which we place in context alongside constraints derived from the Δa_μ , dark matter relic density,¹ and recent Higgs signal strength measurements. Finally, we compare our results with existing bounds from previous studies, including

recent projections from e^-p collider scenarios [9–11], thereby highlighting the complementarity and discovery potential of the e^+e^- collider program in probing ALP scenarios.

After electroweak symmetry breaking, the ALP (a) interacts with a fermionic DM candidate χ via a renormalizable coupling $C_{a\chi}$, while its interactions with the SM charged leptons ℓ and electroweak gauge bosons are described by dimension-5 operators in the effective Lagrangian [1, 9, 10, 12]:

$$\begin{aligned} \mathcal{L}_{\text{eff}}^{\text{int}} \supset & -i \frac{C_{a\chi}}{2} \partial_\mu a \bar{\chi} \gamma^\mu \gamma^5 \chi - \sum_{\ell=e,\mu,\tau} i \frac{C_{\ell\ell}}{2} \frac{\partial_\mu a}{f_a} \bar{\ell} \gamma^\mu \gamma^5 \ell \\ & + e^2 \frac{a}{f_a} g_{\gamma\gamma} F_{\mu\nu} \tilde{F}^{\mu\nu} + \frac{2e^2}{c_w s_w} \frac{a}{f_a} g_{Z\gamma} F_{\mu\nu} \tilde{Z}^{\mu\nu} \\ & + \frac{e^2}{c_w^2 s_w^2} \frac{a}{f_a} g_{ZZ} Z_{\mu\nu} \tilde{Z}^{\mu\nu} + \frac{e^2}{s_w^2} \frac{a}{f_a} g_{WW} W_{\mu\nu} \tilde{W}^{\mu\nu}, \end{aligned} \quad (1)$$

where c_w and s_w are the cosine and the sine of the Weinberg mixing angle θ_w , respectively. For all studies in this work, the scale parameter is fixed at $f_a = 1 \text{ TeV}$. To perform our analysis, we implemented this Lagrangian in FeynRules [13], built the required model files, and used them in our simulations.

2. Analysis & Results

In this section, we present our analysis to derive constraints on the couplings g_{ij} ($i, j = W^\pm, Z, \gamma$) as a function of m_a from the observables at the e^+e^- collider, including Δa_μ , relic density, and the Higgs signal strengths reported in [5–7].

¹Email addresses: pramodsharma.iiser@gmail.com (Pramod Sharma), sohamsingh931@gmail.com (Soham Singh), mukesh.kumar@cern.ch (Mukesh Kumar), agoyal145@yahoo.com (Ashok Goyal)

¹In Ref. [8], the authors explore a new parameter space within a gauged $L_\mu - L_\tau$ extension of the SM that accommodates both the Δa_μ and a viable MeV-scale dark matter candidate.

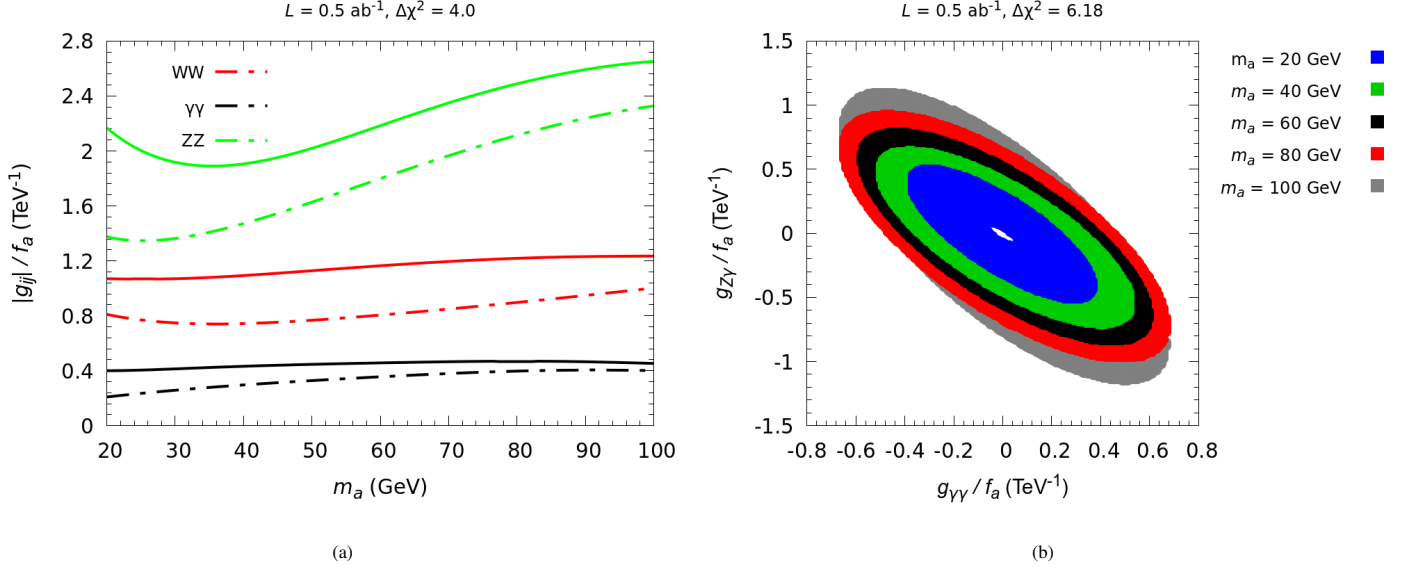


Figure 1: The 95% C.L. exclusion contours with an integrated luminosity of $L = 0.5 \text{ ab}^{-1}$ based on a χ^2 analysis: (a) in the g_{ij}/f_a - m_a plane, using one-bin (solid lines) and multi-bin (dashed lines) approaches, and (b) a two-parameter analysis (with multi-bin) in the $g_{Z\gamma}$ - $g_{\gamma\gamma}$ plane, assuming a fixed coupling of $g_{ZZ} = 0.1$.

2.1. e^+e^- collider:

To estimate constraints on the couplings g_{ij} in a future e^+e^- environment, we consider ALP production via charged-current (CC) (WW -fusion) and neutral-current (NC) processes ($\gamma\gamma$, ZZ , or $Z\gamma$ -fusion), in association with scattered $\nu_e\bar{\nu}_e$ and e^+e^- , respectively. In particular, we focus on the decay $a \rightarrow \gamma\gamma$, with the branching ratio (Br) taken as a function of m_a . In this case, individual couplings are probed by setting $g_{ii} = 1$ while keeping all other couplings at zero. However, for $g_{Z\gamma}$, we set $g_{WW} = 0$, while keeping $g_{\gamma\gamma} \neq 0$ and $g_{ZZ} \neq 0$, so that interference between the $\gamma\gamma$, ZZ , and $Z\gamma$ -fusion channels is taken into account. Note that $\text{Br}(a \rightarrow \gamma\gamma)$ is the dominant decay mode for ALP masses below $m_a < 100 \text{ GeV}$ [11]. The CC and NC signal and corresponding background events, with final states $\nu_e\bar{\nu}_e\gamma\gamma$ and $e^+e^-\gamma\gamma$, respectively, with center-of-mass energy $\sqrt{s} = 250 \text{ GeV}$, are generated using the Monte Carlo event generator package MadGraph5 [14]. Further showering, fragmentation, and hadronization are performed using Pythia8 [15], while detector-level simulation is carried out with Delphes [16], based on the proposed CEPC detector design [17, 18]. The factorization and normalization scales are set to dynamic scale. For this study, e^\pm polarization is taken to be $\pm 80\%$.

At the generation level, nominal selection criteria are imposed, with transverse momentum and rapidity cuts of $p_T^{e^\pm, \gamma} > 10 \text{ GeV}$ and $|\eta^{e^\pm, \gamma}| < 2.5$, respectively. To enhance signal sensitivity against dominant backgrounds, additional analysis-level selections are employed. The di-photon invariant mass is constrained within $|m_{\gamma\gamma} - m_a| < 7.5 \text{ GeV}$. For all channels, the leading photon must satisfy $p_T^\gamma > 20 \text{ GeV}$ for $30 \text{ GeV} < m_a < 50 \text{ GeV}$, and $p_T^\gamma > 30 \text{ GeV}$ for $50 \text{ GeV} < m_a \leq 100 \text{ GeV}$. For the $\gamma\gamma$ and $Z\gamma$ fusion channels, forward-backward rapidity cuts on the scattered e^\pm are applied: $-2.5 < \eta^{e^+} < 0$ and $0 < \eta^{e^-} < 2.5$, while for the ZZ fusion channel, the selection $-1 < \eta^{e^+} < 2.5$ and $-2.5 < \eta^{e^-} < 1$ is imposed. In the WW

fusion channel, a central rapidity requirement of $-1 < \eta^\gamma < 1$ is used, along with a missing transverse energy threshold of $E_T^{\text{miss}} > 20 \text{ GeV}$.

Further, to constrain the ALP-gauge couplings g_{ij} , we perform a χ_N^2 -analysis on optimized events at both the total cross-section level and the most sensitive differential-distribution level.² For CC (NC), the most sensitive differential observable used in the χ_N^2 -analysis is the azimuthal angle difference $\Delta\Phi_{E_T^{\text{miss}}, \gamma_2}$ ($\Delta\Phi_{e^+e^-}$), defined between the missing transverse energy and the sub-leading photon (scattered electron and positron). The χ_N^2 is defined as:

$$\chi_N^2 = \sum_{k=1}^n \left(\frac{N_k(g_{ij}) - N_k^{\text{SM}}}{\Delta N_k} \right)^2, \quad \Delta N_k = \sqrt{N_k^{\text{SM}} (1 + \delta_s^2 N_k^{\text{SM}})}, \quad (2)$$

where $N_k(g_{ij})$ represents the number of signal events in the k^{th} bin of a distribution, with a total of n bins, N_k^{SM} is the corresponding number of background events. For our analysis, we assume $\delta_s = 5\%$ for a given luminosity L , with $L = 0.5 \text{ ab}^{-1}$. The resulting 95% confidence level (C.L.) constraints on g_{ij}/f_a - m_a plane are shown in Figure 1.

2.2. Muon anomalous magnetic moment:

The most recent high-precision measurements of the muon anomalous magnetic moment have been confirmed by several

²To enhance sensitivity to the presence of ALPs in the NC (CC) processes, with $a \rightarrow \gamma\gamma$, we employ as our key observable the azimuthal angle difference between the scattered leptons $\Delta\Phi_{e^+e^-}$ (between the missing transverse momentum and one of the photons, $\Delta\Phi_{E_T^{\text{miss}}, \gamma}$). Since the aVV vertex depends on two independent momenta (p_{V_i}, p_{V_j}), angular observables constructed solely from the decay photons cannot fully capture the underlying coupling structure as they depend only on one momentum p_a combination. In contrast, the fermion lines (scattered e^\pm or E_T^{miss}) retain information about the mediator's momentum flow, hence used as the discriminating observables for the χ_N^2 analysis. This ensures maximal sensitivity to the full Lorentz structure of the effective interaction.

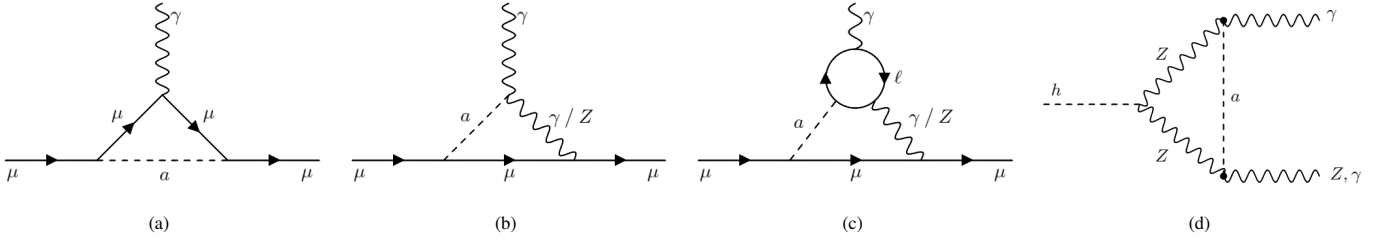


Figure 2: Leading (a), (b) one- and (c) two-loop Feynman diagrams contributing to the muon anomalous magnetic moment, involving an axion-like particle (ALP) and its interactions with SM leptons and neutral electroweak gauge bosons. (d) Feynman diagrams involving ALP couplings $g_{Z\gamma}$ and g_{ZZ} contributing to the loop-induced decays $h \rightarrow Z\gamma$ and $h \rightarrow \gamma\gamma$.

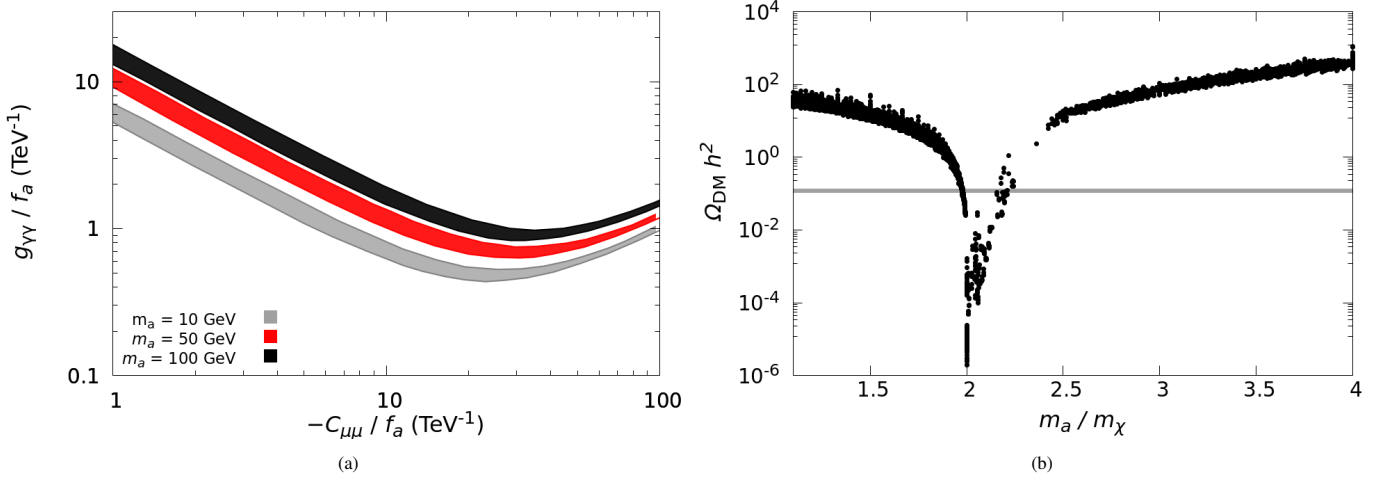


Figure 3: The 4σ contours consistent with the Δa_μ anomaly. (a) Allowed regions in the $(g_{\gamma\gamma}/f_a, C_{\mu\mu}/f_a)$ plane for $m_a = 10, 50$, and 100 GeV. The cutoff scale is set to 1 TeV. (b) Relic density as a function of m_a/m_χ (scatter plot) for couplings that resolve the Δa_μ anomaly. The observed relic density (2σ band) is indicated by the horizontal shaded region, intersecting the curve at two viable values of m_a .

experiments [19], revealing a persistent discrepancy with the SM prediction [20] at the level of approximately 5σ :

$$\Delta a_\mu = a_\mu^{\text{exp}} - a_\mu^{\text{SM}} = (2.49 \pm 0.08) \times 10^{-9}. \quad (3)$$

However, the SM prediction faces tensions between lattice-based calculations of the hadronic vacuum polarization [21, 22] and conservative data-driven estimates from $e^+e^- \rightarrow \text{hadrons}$ cross-section measurements [23]. While ongoing improvements in the SM calculation may reduce the discrepancy with experiment, a resolution remains unconfirmed.

Various beyond the SM (BSM) scenarios have been proposed to explain the Δa_μ anomaly [8, 24–30]. In this work, we focus on contributions from ALPs interacting with charged leptons and electroweak gauge bosons. The leading ALP contributions to Δa_μ arise from both one-loop and two-loop diagrams, as shown in Figure 2. In particular, Figure 2 (a) provides a negative contribution, while Figure 2 (b) and Figure 2 (c) yield positive and negative contributions, respectively, assuming opposite signs for the couplings $C_{\mu\mu}$ and $g_{\gamma\gamma}$ over the m_a range considered in this study. For light ALPs with $0.1 \text{ GeV} \leq m_a \leq 1 \text{ GeV}$, these effects have been studied in [3, 31].

Extending the analysis to higher masses, Figure 3 (a) shows the 4σ region satisfying Δa_μ in the $(g_{\gamma\gamma}/f_a, C_{\mu\mu}/f_a)$ plane for $m_a = 10, 50$, and 100 GeV. As evident from the figure, ac-

commodating Δa_μ within the range $1 \text{ GeV} < m_a < 100 \text{ GeV}$ requires the couplings $g_{\gamma\gamma}/f_a$ and $C_{\mu\mu}/f_a$ to lie in the ranges $\mathcal{O}(10^{-1} - 10^1) \text{ TeV}^{-1}$ and $\mathcal{O}(10^0 - 10^2) \text{ TeV}^{-1}$, respectively.

2.3. Relic-density:

The Planck collaboration has precisely measured the dark matter (DM) relic density, reporting $\Omega_{\text{DM}} h^2 = 0.1198 \pm 0.0012$ [32]. In ALP-portal models, DM candidates can achieve the observed relic density through freeze-out [33, 34], particularly for ALPs in the keV to GeV range and light DM masses $m_\chi < m_a$, where stringent constraints from collider, beam-dump, and astrophysical observations apply [9, 35, 36]. Recently, photon-lepton specific ALPs have also been proposed to address leptonic anomalous magnetic moments in the 0.1 – 1 GeV mass range [3, 31].

In our framework, χ is a fermionic DM particle that interacts with the ALP and remains in thermal equilibrium in the early universe through annihilation channels such as

$$\chi\bar{\chi} \rightarrow \gamma\gamma, \ell\bar{\ell}, Z\gamma, aa, \quad (4)$$

with the $\gamma\gamma$ channel often dominating the cross section. The relic abundance is primarily determined by the thermally averaged annihilation cross section $\langle\sigma v\rangle$, which depends sensitively on the mass hierarchy between χ and the ALP.

For ALP masses in the range $m_a \in [1, 100]$ GeV, two regimes emerge. In the non-resonant regime ($m_\chi < m_a/2$), the channel $\chi\bar{\chi} \rightarrow aa$ is kinematically forbidden, and DM annihilates into SM particles through off-shell ALP exchange, with the cross section scaling as $\langle\sigma v\rangle \sim m_\chi^2/f_a^4$. In the resonant regime ($2m_\chi \sim m_a$), the cross section experiences a Breit-Wigner enhancement via the s -channel resonance, significantly reducing the relic abundance. For $m_\chi > m_a$, the channel $\chi\bar{\chi} \rightarrow aa$ opens up and can dominate, especially when the ALP has sizable decay modes to photons. Constraints from CMB, and indirect detection via gamma rays from *Fermi*-LAT and H.E.S.S., are particularly stringent for light dark matter below the GeV scale [37–42].

For the numerical evaluation of the relic density, we use the package *MicroMEGAS-v6* [43]. Our parameter scan selects points within the 4σ range of the measured Δa_μ (Equation 3). We vary the DM mass in the range $1 \text{ GeV} \leq m_\chi \leq 50 \text{ GeV}$ and scan $C_{a\chi}/f_a$ over the interval $1\text{--}10 \text{ TeV}^{-1}$. In Figure 3 (b), we show the dependence of the relic density on the mass ratio m_a/m_χ , using parameter choices that simultaneously satisfy the Δa_μ anomaly. For a given m_χ , two distinct values of m_a can yield the correct relic abundance while remaining consistent with Δa_μ constraints.

2.4. Higgs signal strength:

Recent measurements by the ATLAS and CMS collaborations report a combined $h \rightarrow Z\gamma$ signal strength of $\mu_{Z\gamma}^{\text{exp}} = 2.2 \pm 0.7$ [5–7], deviating from the SM prediction $\mu_{Z\gamma}^{\text{SM}} = 1$ at the 1.9σ level. While two-loop QCD and electroweak corrections [44–49] refine the SM estimate, they remain insufficient to explain this excess. Due to their loop-induced nature, the $h \rightarrow \gamma\gamma$ (with $\mu_{\gamma\gamma}^{\text{exp}} = 1.10 \pm 0.06$ [50]) and $h \rightarrow Z\gamma$ decay channels are highly sensitive to new physics. In particular, ALP contributions at one loop [51] can significantly modify these rates via effective couplings $g_{\gamma\gamma}$ and $g_{Z\gamma}$, as illustrated in Figure 2 (d).

The modified Higgs signal strength due to BSM effects is defined as

$$\mu_{XY}^{\text{BSM}} = \frac{\Gamma_{\text{BSM}}(h \rightarrow XY)}{\Gamma_{\text{SM}}(h \rightarrow XY)}, \quad (5)$$

where $XY = \gamma\gamma$ or $Z\gamma$, and Γ_{BSM} includes ALP-induced loop contributions. To constrain the ALP couplings, we construct a $\Delta\chi_\mu^2$ estimator,

$$\Delta\chi_\mu^2 = \left(\frac{\mu_{XY}^{\text{BSM}} - \mu_{XY}^{\text{exp}}}{\Delta\mu_{XY}^{\text{exp}}} \right)^2, \quad (6)$$

and apply a 2σ bound, taking $\Delta\chi^2 = 4.0$ for single-parameter fits and $\Delta\chi^2 = 6.18$ for two-parameter fits.

For each ALP mass m_a in the range 1–100 GeV, we first determine the values of $g_{\gamma\gamma}/f_a$ vs m_a that satisfy the Δa_μ anomaly within 4σ . Independently, we compute the allowed $g_{Z\gamma}/f_a$ range using the measured $\mu_{\gamma\gamma}^{\text{exp}}$, applying a one-parameter $\Delta\chi_\mu^2$ test with a 2σ constraint. Combining these results, we scan over the $(g_{\gamma\gamma}/f_a, g_{Z\gamma}/f_a)$ plane and evaluate the consistency of each parameter point with the measured $\mu_{Z\gamma}^{\text{exp}}$ using the two-parameter $\Delta\chi_\mu^2$ test. For this calculation, the cutoff scale is set to $4\pi f_a$.

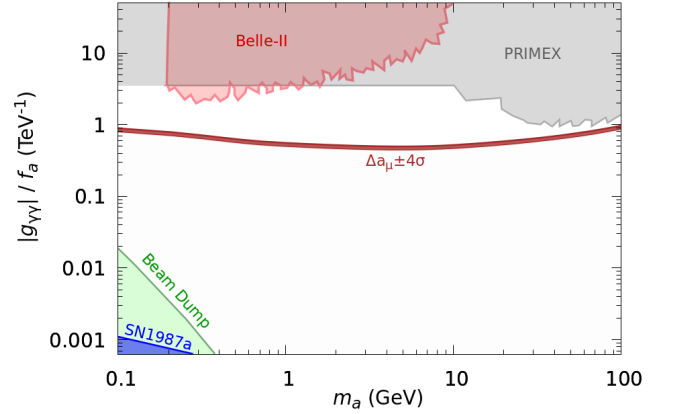


Figure 4: Allowed parameter space in the $g_{\gamma\gamma}/f_a - m_a$ plane. The brown band represents the 4σ region favored by the Δa_μ anomaly, for which the entire parameter space also satisfies the dark matter relic density and the experimental measurement of $\mu_{Z\gamma}^{\text{exp}}$ within 2σ . A uniform bound of $|g_{Z\gamma}|/f_a < 0.7 \text{ TeV}^{-1}$, derived from Higgs signal strength measurements [5–7], is imposed across the full m_a range. Additional experimental constraints from PRIMEX [52], Belle-II [53], beam dump experiments, and SN1987A [54, 55] are shown for comparison. The region with $m_a < 1 \text{ GeV}$ is shown only for comparison, where the Δa_μ anomaly is satisfied within 4σ and $\mu_{Z\gamma}^{\text{exp}}$ within 2σ ; relic density constraints are not applied in this range.

In Figure 4, we show the allowed parameter space in the $g_{\gamma\gamma}/f_a - m_a$ plane. The brown band corresponds to the 4σ region favored by the Δa_μ anomaly, for which the entire parameter space simultaneously satisfies the dark matter relic density and the experimental measurement of $\mu_{Z\gamma}^{\text{exp}}$ within 2σ . Notably, for the $g_{Z\gamma}$ coupling, a uniform bound of $|g_{Z\gamma}|/f_a < 0.7 \text{ TeV}^{-1}$ is observed across the entire mass range of m_a , and this constraint is therefore imposed as an additional bound. The coupling $C_{\mu\mu}/f_a$ is of order $O(10^1) \text{ TeV}^{-1}$.

3. Discussion and conclusions

The objective of this article was to present a coherent two-step framework to constrain Axion-Like Particle (ALP) couplings. First, we obtained independent bounds on the couplings $g_{\gamma\gamma}$, g_{ZZ} , $g_{Z\gamma}$, and g_{WW} using projected sensitivities at an e^+e^- collider with $\sqrt{s} = 250 \text{ GeV}$ and integrated luminosity of 0.5 ab^{-1} for $m_a \in [20, 100] \text{ GeV}$. In the second step, we focused on the 4σ region favored by the Δa_μ anomaly, and identified the subset of this region that also satisfies the observed dark matter relic density and the Higgs signal strengths $\mu_{\gamma\gamma}$ and $\mu_{Z\gamma}$ within 2σ , thereby yielding tighter constraints on $g_{\gamma\gamma}/f_a$ over the mass range $1 \text{ GeV} \leq m_a \leq 100 \text{ GeV}$. The constraints shown in Figure 1 and Figure 4 are obtained from two complementary analyses. Both yield a limit of order $O(10^{-1}) \text{ TeV}^{-1}$ on $g_{\gamma\gamma}/f_a$, assuming $f_a = 1 \text{ TeV}$.

To compare the obtained limits, the 95% C.L. contours in the $|g_{ij}|/f_a - m_a$ plane are shown in Figure 5. The solid brown line corresponds to constraints from the e^+e^- collider analysis, while the dashed brown line represents the most conservative bounds derived solely from the Higgs signal strength $\mu_{\gamma\gamma, Z\gamma}^{\text{exp}}$ analysis. To extract limits on g_{ZZ} , $g_{Z\gamma}$, and g_{WW} from $g_{\gamma\gamma}$ using the $\mu_{\gamma\gamma, Z\gamma}^{\text{exp}}$

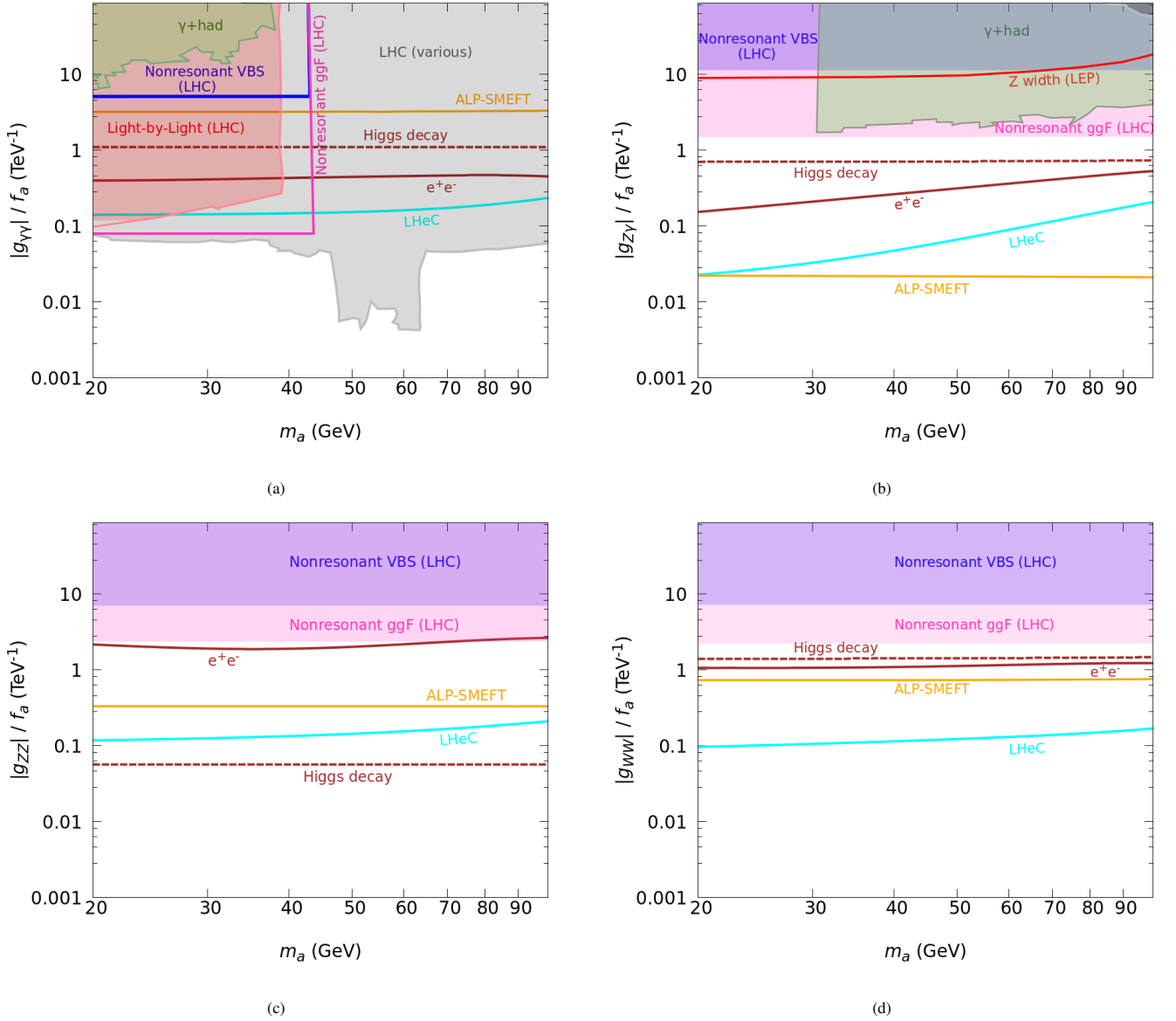


Figure 5: The 95% C.L. exclusion contours in the $|g_{ij}|/f_a - m_a$ plane obtained from a multiple-bin χ^2 analysis at e^+e^- collider with $L = 0.5 \text{ ab}^{-1}$. Limits from LHC, γ +hadron searches, Z-width at LEP, and ALP-SMEFT interpretations are shown for comparison [9, 10, 12, 56–67]. The solid *brown* line shows our result from e^+e^- analysis; the dashed *brown* line corresponds to constraints from $\mu_{\gamma\gamma, Z\gamma}^{\text{exp}}$ -based analysis under a conservative assumption. For $g_{Z\gamma}$, interference effects with $g_{\gamma\gamma}$ and g_{ZZ} are accounted for; a standalone limit is shown for $g_{\gamma\gamma} = 0.1 = g_{ZZ}$. The LHeC limits with $L = 1 \text{ ab}^{-1}$ are adopted from Ref. [11].

analysis, we employ the relations [11]:

$$g_{Z\gamma} = g_{WW} - s_w^2 g_{\gamma\gamma}, \quad g_{ZZ} = (c_w^2 - s_w^2) g_{WW} + s_w^4 g_{\gamma\gamma}. \quad (7)$$

At 95% C.L., the e^+e^- collider provides stronger constraints on $g_{\gamma\gamma}/f_a$ —at the level of $\mathcal{O}(10^{-1}) \text{ TeV}^{-1}$, than those obtained from Higgs decay measurements $h \rightarrow \gamma\gamma$ and $h \rightarrow Z\gamma$. Constraints on $g_{Z\gamma}$ are correlated with $g_{\gamma\gamma}$ and g_{ZZ} due to interference; for an isolated comparison, we fix $g_{\gamma\gamma} = 0.1$ and $g_{ZZ} = 0.1$. The $g_{Z\gamma}/f_a$ bounds from both Higgs and e^+e^- analyses are at $\mathcal{O}(10^{-1}) \text{ TeV}^{-1}$. For g_{ZZ}/f_a , Higgs data constrains it to $\mathcal{O}(10^{-1}) \text{ TeV}^{-1}$, whereas e^+e^- reaches $\mathcal{O}(10^0) \text{ TeV}^{-1}$. The g_{WW}/f_a limits from both sources lie around $\mathcal{O}(10^0) \text{ TeV}^{-1}$.

These findings demonstrate that precision measurements at future e^+e^- colliders can probe ALP couplings with a sensitivity

comparable to or exceeding that of current Higgs signal strength constraints. In particular, the collider setup offers complementary and, in some cases, stronger limits on g_{ij}/f_a , especially for $g_{\gamma\gamma}$ and $g_{Z\gamma}$. The coherent two-step approach outlined here provides a robust framework to test ALP scenarios motivated by the Δa_μ anomaly, dark matter relic abundance, and Higgs phenomenology. These constraints are obtained from full detector-level simulations with a conservative 5% systematic uncertainty, reinforcing the robustness of the projections. This underscores the role of e^+e^- machines as precision tools for ALP coupling reconstruction across a broad mass range.

References

- [1] Howard Georgi, David B. Kaplan, and Lisa Randall. Manifesting the Invisible Axion at Low-energies. *Phys. Lett. B*, 169:73–78, 1986.
- [2] Mohapatra R. N. Chikashige, Y. and R. D. Peccei. Are There Real Goldstone Bosons Associated with Broken Lepton Number? *Phys. Lett. B*, 98:265–268, 1981.
- [3] W. J. Marciano, A. Masiero, P. Paradisi, and M. Passera. Contributions of axionlike particles to lepton dipole moments. *Phys. Rev. D*, 94(11):115033, 2016.
- [4] Eder Izaguirre, Yonatan Kahn, Gordan Krnjaic, and Matthew Moschella. Testing Light Dark Matter Coannihilation With Fixed-Target Experiments. *Phys. Rev. D*, 96(5):055007, 2017.
- [5] Georges Aad et al. A search for the $Z\gamma$ decay mode of the Higgs boson in pp collisions at $\sqrt{s} = 13$ TeV with the ATLAS detector. *Phys. Lett. B*, 809:135754, 2020.
- [6] Armen Tumasyan et al. Search for Higgs boson decays to a Z boson and a photon in proton-proton collisions at $\sqrt{s} = 13$ TeV. *JHEP*, 05:233, 2023.
- [7] Georges Aad et al. Evidence for the Higgs Boson Decay to a Z Boson and a Photon at the LHC. *Phys. Rev. Lett.*, 132(2):021803, 2024.
- [8] Ian Holst, Dan Hooper, and Gordan Krnjaic. Simplest and Most Predictive Model of Muon $g-2$ and Thermal Dark Matter. *Phys. Rev. Lett.*, 128(14):141802, 2022.
- [9] Martin Bauer, Matthias Neubert, and Andrea Thamm. Collider Probes of Axion-Like Particles. *JHEP*, 12:044, 2017.
- [10] I. Brivio, M. B. Gavela, L. Merlo, K. Mimasu, J. M. No, R. del Rey, and V. Sanz. ALPs Effective Field Theory and Collider Signatures. *Eur. Phys. J. C*, 77(8):572, 2017.
- [11] Karabo Mosala, Pramod Sharma, Mukesh Kumar, and Ashok Goyal. Axion-like particles at future e^+e^- collider. *Eur. Phys. J. C*, 84(1):44, 2024.
- [12] Martin Bauer, Mathias Heiles, Matthias Neubert, and Andrea Thamm. Axion-Like Particles at Future Colliders. *Eur. Phys. J. C*, 79(1):74, 2019.
- [13] Adam Alloul, Neil D. Christensen, Céline Degrande, Claude Duhr, and Benjamin Fuks. FeynRules 2.0 - A complete toolbox for tree-level phenomenology. *Comput. Phys. Commun.*, 185:2250–2300, 2014.
- [14] Johan Alwall, Michel Herquet, Fabio Maltoni, Olivier Mattelaer, and Tim Stelzer. MadGraph 5 : Going Beyond. *JHEP*, 06:128, 2011.
- [15] Torbjorn Sjostrand, Stephen Mrenna, and Peter Z. Skands. A Brief Introduction to PYTHIA 8.1. *Comput. Phys. Commun.*, 178:852–867, 2008.
- [16] J. de Favereau, C. Delaere, P. Demin, A. Giammanco, V. Lemaître, A. Mertens, and M. Selvaggi. DELPHES 3, A modular framework for fast simulation of a generic collider experiment. *JHEP*, 02:057, 2014.
- [17] Cheng Chen, Xin Mo, Michele Selvaggi, Qiang Li, Gang Li, Manqi Ruan, and Xinchou Lou. Fast simulation of the CEPC detector with Delphes. 12 2017.
- [18] Waleed Abdallah et al. CEPC Technical Design Report – Accelerator (v2). 12 2023.
- [19] D. P. Aguillard et al. Measurement of the Positive Muon Anomalous Magnetic Moment to 0.20 ppm. *Phys. Rev. Lett.*, 131(16):161802, 2023.
- [20] T. Aoyama et al. The anomalous magnetic moment of the muon in the Standard Model. *Phys. Rept.*, 887:1–166, 2020.
- [21] A. Boccaletti et al. High precision calculation of the hadronic vacuum polarisation contribution to the muon anomaly. 7 2024.
- [22] Simon Kuberski. Muon $g - 2$: Lattice calculations of the hadronic vacuum polarization. *PoS, LATTICE2023*:125, 2024.
- [23] Alexander Keshavarzi, Daisuke Nomura, and Thomas Teubner. $g - 2$ of charged leptons, $\alpha(M_Z^2)$, and the hyperfine splitting of muonium. *Phys. Rev. D*, 101(1):014029, 2020.
- [24] Ashok Goyal, Mohammed Omer Khojali, Mukesh Kumar, and Alan S. Cornell. Neutrino specific spin-3/2 dark matter. *Eur. Phys. J. C*, 82(11):1002, 2022.
- [25] Danielle Sabatta, Alan S. Cornell, Ashok Goyal, Mukesh Kumar, Bruce Mellado, and Xifeng Ruan. Connecting muon anomalous magnetic moment and multi-lepton anomalies at LHC. *Chin. Phys. C*, 44(6):063103, 2020.
- [26] Peter Athron, Csaba Balázs, Douglas H. J. Jacob, Wojciech Kotlarski, Dominik Stöckinger, and Hyejung Stöckinger-Kim. New physics explanations of a_μ in light of the FNAL muon $g - 2$ measurement. *JHEP*, 09:080, 2021.
- [27] Rodolfo Capdevilla, David Curtin, Yonatan Kahn, and Gordan Krnjaic. No-lose theorem for discovering the new physics of $(g - 2)_\mu$ at muon colliders. *Phys. Rev. D*, 105(1):015028, 2022.
- [28] Hrishabh Bharadwaj, Sukanta Dutta, and Ashok Goyal. Leptonic $g - 2$ anomaly in an extended Higgs sector with vector-like leptons. *JHEP*, 11:056, 2021.
- [29] Patrick Foldenauer. Light dark matter in a gauged $U(1)_{L_\mu - L_\tau}$ model. *Phys. Rev. D*, 99(3):035007, 2019.
- [30] Manuel Drees and Wenbin Zhao. $U(1)_{L_\mu - L_\tau}$ for light dark matter, $g\mu - 2$, the 511 keV excess and the Hubble tension. *Phys. Lett. B*, 827:136948, 2022.
- [31] Wai-Yee Keung, Danny Marfatia, and Po-Yan Tseng. Axion-Like Particles, Two-Higgs-Doublet Models, Leptoquarks, and the Electron and Muon $g - 2$. *LHEP*, 2021:209, 2021.
- [32] N. Aghanim et al. Planck 2018 results. VI. Cosmological parameters. *Astron. Astrophys.*, 641:A6, 2020. [Erratum: *Astron. Astrophys.* 652, C4 (2021)].
- [33] Matthew J. Dolan, Torben Ferber, Christopher Hearty, Felix Kahlhoefer, and Kai Schmidt-Hoberg. Revised constraints and Belle II sensitivity for visible and invisible axion-like particles. *JHEP*, 12:094, 2017. [Erratum: *JHEP* 03, 190 (2021)].
- [34] Luc Darmé, Federica Giacchino, Enrico Nardi, and Mauro Raggi. Invisible decays of axion-like particles: constraints and prospects. *JHEP*, 06:009, 2021.
- [35] Jae Hyeok Chang, Rouven Essig, and Samuel D. McDermott. Supernova 1987A Constraints on Sub-GeV Dark Sectors, Millicharged Particles, the QCD Axion, and an Axion-like Particle. *JHEP*, 09:051, 2018.
- [36] Ken Mimasu and Verónica Sanz. ALPs at Colliders. *JHEP*, 06:173, 2015.
- [37] Planck Collaboration, N. Aghanim, et al. Planck 2018 results. VI. Cosmological parameters. *Astronomy & Astrophysics*, 641:A6, 2020.
- [38] Tracy R. Slatyer. Energy injection and absorption in the cosmic dark ages. *Phys. Rev. D*, 87:123513, 2013.
- [39] Fermi-LAT Collaboration. Searching for dark matter annihilation from milky way dwarf spheroidal galaxies with six years of fermi data. *Phys. Rev. Lett.*, 115:231301, 2015.
- [40] H.E.S.S. Collaboration. Search for gamma-ray line signals from dark matter annihilations in the inner galactic halo from ten years of observations with h.e.s.s. *Phys. Rev. Lett.*, 120:201101, 2018.
- [41] *Fundamental Physics at the Intensity Frontier*, 5 2012.
- [42] P. A. R. Ade et al. Planck 2013 results. XV. CMB power spectra and likelihood. *Astron. Astrophys.*, 571:A15, 2014.
- [43] G. Alguero, G. Belanger, F. Boudjema, S. Chakraborti, A. Goudelis, S. Kraml, A. Mjallal, and A. Pukhov. micrOMEGAs 6.0: N-component dark matter. *Comput. Phys. Commun.*, 299:109133, 2024.
- [44] M. Spira, A. Djouadi, and P. M. Zerwas. QCD corrections to the H Z gamma coupling. *Phys. Lett. B*, 276:350–353, 1992.
- [45] Thomas Gehrmann, Sam Guns, and Dominik Kara. The rare decay $H \rightarrow Z\gamma$ in perturbative QCD. *JHEP*, 09:038, 2015.
- [46] Federico Buccioni, Federica Devoto, Abdelhak Djouadi, John Ellis, Jérémie Quevillon, and Lorenzo Tancredi. Interference effects in $g\bar{g}H\bar{B}Z\gamma$ beyond leading order. *Phys. Lett. B*, 851:138596, 2024.
- [47] R. Bonciani, Vittorio Del Duca, Hjalte Frellesvig, Johannes M. Henn, Francesco Moriello, and Vladimir A. Smirnov. Next-to-leading order QCD corrections to the decay width $H \rightarrow Z\gamma$. *JHEP*, 08:108, 2015.
- [48] Zi-Qiang Chen, Long-Bin Chen, Cong-Feng Qiao, and Ruilin Zhu. Two-loop electroweak corrections to the Higgs boson rare decay process $H\bar{B}Z\gamma$. *Phys. Rev. D*, 110(5):L051301, 2024.
- [49] Wen-Long Sang, Feng Feng, and Yu Jia. Next-to-leading-order electroweak correction to $H\bar{B}Z^0\gamma$. *Phys. Rev. D*, 110(5):L051302, 2024.
- [50] S. Navas et al. Review of particle physics. *Phys. Rev. D*, 110(3):030001, 2024.
- [51] Masashi Aiko and Motoi Endo. Higgs probes of axion-like particles. *JHEP*, 11:046, 2023.
- [52] Daniel Aloni, Cristiano Fanelli, Yotam Soreq, and Mike Williams. Photo-production of Axionlike Particles. *Phys. Rev. Lett.*, 123(7):071801, 2019.
- [53] F. Abudinén et al. Search for Axion-Like Particles produced in e^+e^- collisions at Belle II. *Phys. Rev. Lett.*, 125(16):161806, 2020.
- [54] Manuel A. Buen-Abad, JiJi Fan, Matthew Reece, and Chen Sun. Challenges for an axion explanation of the muon $g - 2$ measurement. *JHEP*, 09:101, 2021.
- [55] Prateek Agrawal et al. Feebly-interacting particles: FIPs 2020 workshop report. *Eur. Phys. J. C*, 81(11):1015, 2021.

- [56] O. Adriani et al. Isolated hard photon emission in hadronic Z^0 decays. *Phys. Lett. B*, 292:472–484, 1992.
- [57] Joerg Jaeckel, Martin Jankowiak, and Michael Spannowsky. LHC probes the hidden sector. *Phys. Dark Univ.*, 2:111–117, 2013.
- [58] Alberto Mariotti, Diego Redigolo, Filippo Sala, and Kohsaku Tobioka. New LHC bound on low-mass diphoton resonances. *Phys. Lett. B*, 783:13–18, 2018.
- [59] Albert M Sirunyan et al. Evidence for light-by-light scattering and searches for axion-like particles in ultraperipheral PbPb collisions at $\sqrt{s_{NN}} = 5.02$ TeV. *Phys. Lett. B*, 797:134826, 2019.
- [60] Georges Aad et al. Measurement of light-by-light scattering and search for axion-like particles with 2.2 nb^{-1} of Pb+Pb data with the ATLAS detector. *JHEP*, 03:243, 2021. [Erratum: *JHEP* 11, 050 (2021)].
- [61] Nathaniel Craig, Anson Hook, and Skyler Kasko. The Photophobic ALP. *JHEP*, 09:028, 2018.
- [62] M. B. Gavela, J. M. No, V. Sanz, and J. F. de Trocóniz. Nonresonant Searches for Axionlike Particles at the LHC. *Phys. Rev. Lett.*, 124(5):051802, 2020.
- [63] Sonia Carra, Vincent Goumarre, Ruchi Gupta, Sarah Heim, Beate Heine-
mann, Jan Kuechler, Federico Meloni, Pablo Quilez, and Yee-Chinn Yap. Constraining off-shell production of axionlike particles with $Z\gamma$ and WW differential cross-section measurements. *Phys. Rev. D*, 104(9):092005, 2021.
- [64] Armen Tumasyan et al. Search for heavy resonances decaying to ZZ or ZW and axion-like particles mediating nonresonant ZZ or ZH production at $\sqrt{s} = 13$ TeV. *JHEP*, 04:087, 2022.
- [65] J. Bonilla, I. Brivio, J. Machado-Rodríguez, and J. F. de Trocóniz. Nonresonant searches for axion-like particles in vector boson scattering processes at the LHC. *JHEP*, 06:113, 2022.
- [66] G. Alonso-Álvarez, M. B. Gavela, and P. Quilez. Axion couplings to electroweak gauge bosons. *Eur. Phys. J. C*, 79(3):223, 2019.
- [67] Anke Biekötter, Javier Fuentes-Martín, Anne Mareike Galda, and Matthias Neubert. A global analysis of axion-like particle interactions using SMEFT fits. *JHEP*, 09:120, 2023.